Libraries and Learning Services

University of Auckland Research Repository, ResearchSpace

Version

This is the publisher's version. This version is defined in the NISO recommended practice RP-8-2008 http://www.niso.org/publications/rp/

Suggested Reference

Copyright

In vivo spinal nerve sensing in MISS using Raman spectroscopy

Hao Chen*[a,c], Weiliang Xu [a,c], Neil Broderick[b,c]
[a]Department of Mechanical Engineering, the University of Auckland, Auckland, New Zealand;
[b]Department of Physics, the University of Auckland, Auckland, New Zealand; [c]The Dodd-Walls Center for Photonic and Quantum Technologies, New Zealand

ABSTRACT

In modern Minimally Invasive Spine Surgery (MISS), lack of visualization and haptic feedback information are the main obstacles. The spinal cord is a part of the central nervous system (CNS). It is a continuation of the brain stem, carries motor and sensory messages between CNS and the rest of body, and mediates numerous spinal reflexes. Spinal cord and spinal nerves are of great importance but vulnerable, once injured it may result in severe consequences to patients, e.g. paralysis. Raman Spectroscopy has been proved to be an effective and powerful tool in biological and biomedical applications as it works in a rapid, non-invasive and label-free way. It can provide molecular vibrational features of tissue samples and reflect content and proportion of protein, nucleic acids lipids etc. Due to the distinct chemical compositions spinal nerves have, we proposed that spinal nerves can be identified from other types of tissues by using Raman spectroscopy. Ex vivo experiments were first done on samples taken from swine backbones. Comparative spectral data of swine spinal cord, spinal nerves and adjacent tissues (i.e. membrane layer of the spinal cord, muscle, bone and fatty tissue) are obtained by a Raman micro-spectroscopic system and the peak assignment is done. Then the average spectra of all categories of samples are averaged and normalized to the same scale to see the difference against each other. The results verified the feasibility of spinal cord and spinal nerves identification by using Raman spectroscopy. Besides, a fiber-optic Raman sensing system including a miniature Raman sensor for future study is also introduced. This Raman sensor can be embedded into surgical tools for MISS.

Keywords: Nerve sensing, Raman spectroscopy, Raman probe, Spinal nerve identification, Minimally Invasive Spine Surgery, MISS

1. INTRODUCTION

Minimally Invasive Spine Surgery (MISS), take advantage of several small-sized keyhole incisions (usually 3 to 5 mm) for surgeons to conduct various treatment operations for different types of spine diseases or abnormal conditions, such as spine fractures, intervertebral disc herniation, tumors and spine deformities[1]. Compared with traditional open spine surgery, patients can benefit enormously in terms of shorter postoperative hospitalization and recovery time, less tissue damage and blood loss[2, 3]. However, at the same time, MISS also has its limitations. Due to the decreased feedback information and limited visualization, it may bring much more difficulties for surgeons to conduct precise surgical manipulations and avoid damaging fragile but important tissues[4]. Serious consequence might happen if surgical instruments were placed in a wrong position or other mishandling due to the limitation of MISS.

The spinal cord, a part of central nervous system (CNS), works as a massage pathway to connect the brain with the rest of the body. It passes all the movement instructions from the brain to other parts of body and in return carries feeling information from body parts to the brain. Due to the current MISS environment, iatrogenic spinal cord injury (SCI) is not a rare phenomenon in the operation theater. Efforts have been made towards reducing the incidence of iatrogenic SCI happens during MISS. Intraoperative image guidance techniques like fluoroscopy are frequently used to guide surgical instruments or locate the target lesion. However, in the meantime, these techniques have obvious disadvantages: indirect, time-consuming, and ambiguity of the observed images. Intraoperative neural monitoring systems are another applied techniques in the operation room. They can either monitor the motor evoked potentials[5] (MEP), somatosensory evoked potentials[6] (SEP), or combine these with other techniques. However, these neural monitoring systems work only after certain injuries happen to the spinal cord. They are not able to predict and prevent the spinal cord from being injured. Thus, there is a need to develop a sensor which is capable of detect the spinal cord or spinal nerves before injury take place on them.

*hche958@aucklanduni.ac.nz; phone 64 22 631 4012.

Raman spectroscopy (RS), based on measuring the inelastic scattering light which contains detailed chemical composition and molecular vibrational information about the sample, has become a highly valuable and powerful analytical tool in bio-medical and clinical applications[7]. Each chemical bond within a sample has an exclusive molecular structure which can be reflected in a Raman spectrum called as its molecular "fingerprints". Due to different types of tissue samples have different chemical compositions, Raman spectroscopy is able to identify the types of the tissue under investigated. Besides, it can also detect the bio-molecular changes within the same type of tissue which makes it possible to detect and characterize diseases, including cancers and other pathologies[8]. Many research groups have successfully applied Raman spectroscopy to detect cancerous changes in different organs, such as brain[9], esophagus[10], bladder[11] etc.

Compared with infrared spectroscopy (IR), which is commonly considered to be complementary with RS, RS has many important advantages especially for in vivo applications over IR. The most significant one is RS is able to perform measurement in a confined space deep inside the body by utilizing fiber optics[12]. Besides, water has a strong absorption for IR, whereas it has little influence to RS. And these advantages make RS more suitable for in vivo spinal cord and spinal nerves identification.

Our research intends to develop a miniature fiber-optic Raman sensor for in vivo spinal cord and spinal nerve detection in MISS. And this Raman sensor is capable of being embedded into certain surgical tools which are often used in the operation theatre, like a puncture needle or a surgical cannula. In this paper, only the preliminary work of this research will be described, i.e. Raman microscope experiments to demonstrate the feasibility of this research. The experiment results can also work as benchmark or reference for the future Raman sensor experiment.

2. METHODS

2.1 Mechanism of Raman spectroscopy

Raman scattering effect was first introduced by C. V. Raman and K. S. Krishnan in 1928[13]. The principle of Raman spectroscopy is based on measuring inelastic scattered light or photons. To be more exact, Raman spectroscopy usually uses a monochromatic laser light as incident light source. Most of the excitation photons are scattered elastically into all directions without energy exchange and this effect is called as Rayleigh scattering. Some other incident photons are absorbed by the molecules of the sample and then re-emit by the sample which generate the effect of fluorescence. However, a very little proportion of incident light, about 1 in 10^6 to 10^8 photons, will experience inelastic scattering, and this effect is noted as Raman scattering. The inelastically scattered photon may have an energy difference compared with the incident light. If the scattered photon possesses higher energy than the incident photon, it results in an anti-Stokes Raman shift, which is also called "blue shift"; If the scattered photon has a lower energy after the scattering, it relates to a Stokes Raman shift, which is also called "red shift". This Raman scattered light contains information about the vibrational modes of the molecule of the sample. Figure. 1 illustrates the light scattering mechanism of Raman spectroscopy.
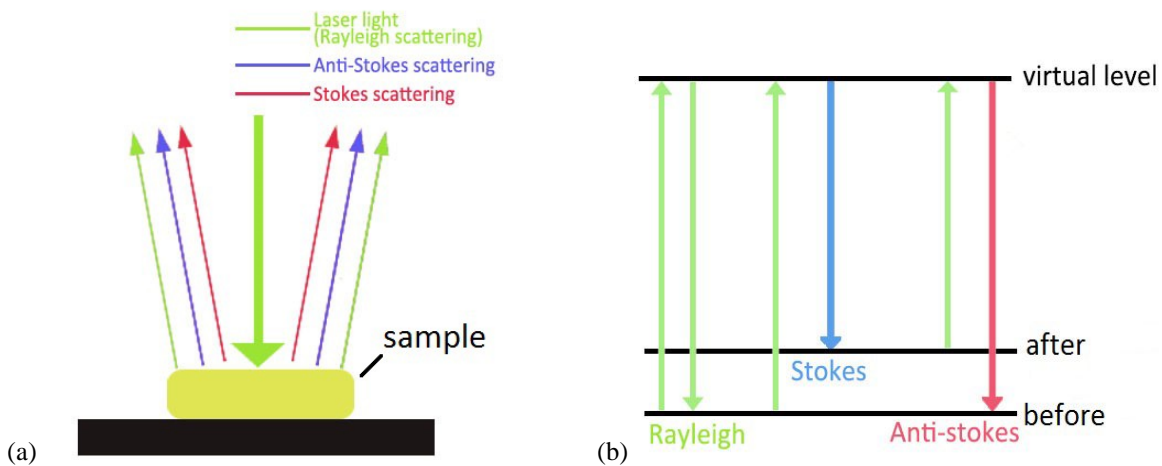
Figure. 1 Mechanism of Raman spectroscopy. (a) Light scattering when laser light incident on a sample; (b) the energy difference of target molecule before and after scattering.

2.2 Fiber-optic Raman sensing system setup

Although the Raman sensor experiment will not be described, the basic fiber-optic Raman sensing system setup for future experiments will be introduced in this section. Briefly, the entire system consists of a continuous 785 nm near-infrared (NIR) laser source (FC-D-785, 0 to 450 mW adjustable, X2 Labwares Priveate Limited, Singapore), a miniature fiber-optic Raman sensor, a compact spectrometer (TG-Raman 785 -1100 nm, X2 Labwares Private Limited, Singapore), and a computer with certain software to do data analyzing. This Raman sensor can be embedded into surgical tools like a surgical cannula which is often used in minimally invasive spine surgeries like vertebroplasty or discectomy.

2.3 Raman microscope experiment

Materials: the biological tissue samples we use for the Raman microscope experiment are porcine tissue samples taken from swine backbone. They are divided into five categories: the spinal cord samples, membrane layer of the spinal cord, muscle samples, bone tissue samples and fatty tissue samples. The samples are made thick enough so that the laser light will not penetrate through.

Instrumentation: Renishaw RM1000 Raman microscope system. The RM1000 is equipped with an air cooled Argon ion 488nm excitation laser and solid state diode 785 nm excitation laser. Actually, only the 785 nm laser is applied since biological samples are strongly fluorescent. The power of the laser is tuned to 10% of full power (about 115 W/m^2 at the sample with a 50x objective) to lower the fluorescence background and increase the signal to background ratio (SBR). The time of each scan is set as 30 s and 10 accumulations for each spectrum, which means about taking 5 mins for each spectrum. Ten spectra for each category of samples are taken and the average spectra are calculated. Before taking measurement on tissue samples, we use the peak of calcite at 1086 cm^{-1} to do the spectrum calibration for this Raman microscope. The spectral range is from 200 to 2000 cm^{-1}.

3. RESULTS AND DISCUSSION

After took 10 measurements on each category of samples, first the fluorescence background of each spectrum is subtracted by using a 4-th order polynomial fitting. Then the average spectra are calculated and the results are shown in Figure 2. The Raman peak assignments used in this paper are summarized in Table 1.

The spinal cord contains two main structures: the grey matter and the white matter. The grey matter in the middle of the spinal cord has a butterfly shape and contains millions of motor and sensory neurons. The white matter locates outside of the grey matter containing the axons originated from the neurons. And most of the axons are myelinated nerve fibers making the spinal cord a lipid-rich tissue. As can be seen from Figure 2(a), the characteristic Raman peaks of swine spinal cord can be found at 418, 548, 608, 702, 719, 847, 870, 1004, 1064, 1129, 1298, 1438, and 1659 cm^{-1} in the finger print region. Among these, peaks at 870, 1064, 1129, 1438 and 1659 cm^{-1} are assigned to lipids or phospholipids; 548, 608, 702 cm^{-1} are assigned to cholesterol; Peaks at 1298 and 1659 cm^{-1} are assigned to fatty acid and protein respectively.

The membrane layer or the sheath of the spinal cord consists of three layers the same as the brain does: dura matter, arachnoid mater and pia matter. Dura matter is the toughest and outermost layer to protect the spinal cord. Pia matter adheres to the surface of the spinal cord. And the arachnoid matter stays between the dura matter and pia matter. The characteristic peaks of the membrane layer of the spinal cord are 418, 643, 847, 870, 1004 and 1620 cm^{-1} which is shown in Figure 2(b). The spectrum of the membrane layer is similar to that of muscle tissues and they both experience strong fluorescence from 1000 to 1700 cm^{-1}.

Bone tissues or osseous tissues contains plenty of calcium hydroxylapatite. The average spectrum of bone is shown in Figure 2(d). There is a strong peak at 960 cm^{-1} which reflects the contents of calcium hydroxyapatite. And peaks at 1073 and 1448 cm^{-1} can also be assigned to this compound. Other peaks at 856 and 1658 cm^{-1} can be assigned to collagen and Amide I vibration of proteins.

The main cells in fatty tissue are adipocytes. The chemical compositions of fatty tissue are lipids, cholesterol, cholesterol ester, fatty acid, and unsaturated fatty acid[14]. Figure 2(e) shows the average spectrum of swine fatty tissue taken from swine backbones. The characteristic peaks are at 418, 847, 870, 890, 1063, 1129, 1298, 1440, 1655 and 1743 cm^{-1}. Peaks at 418 and 1298 cm^{-1} reflect the contents of Cholesterol and fatty acid. Peaks at 870, 1063, 1129, and 1743 indicate the content of lipids.
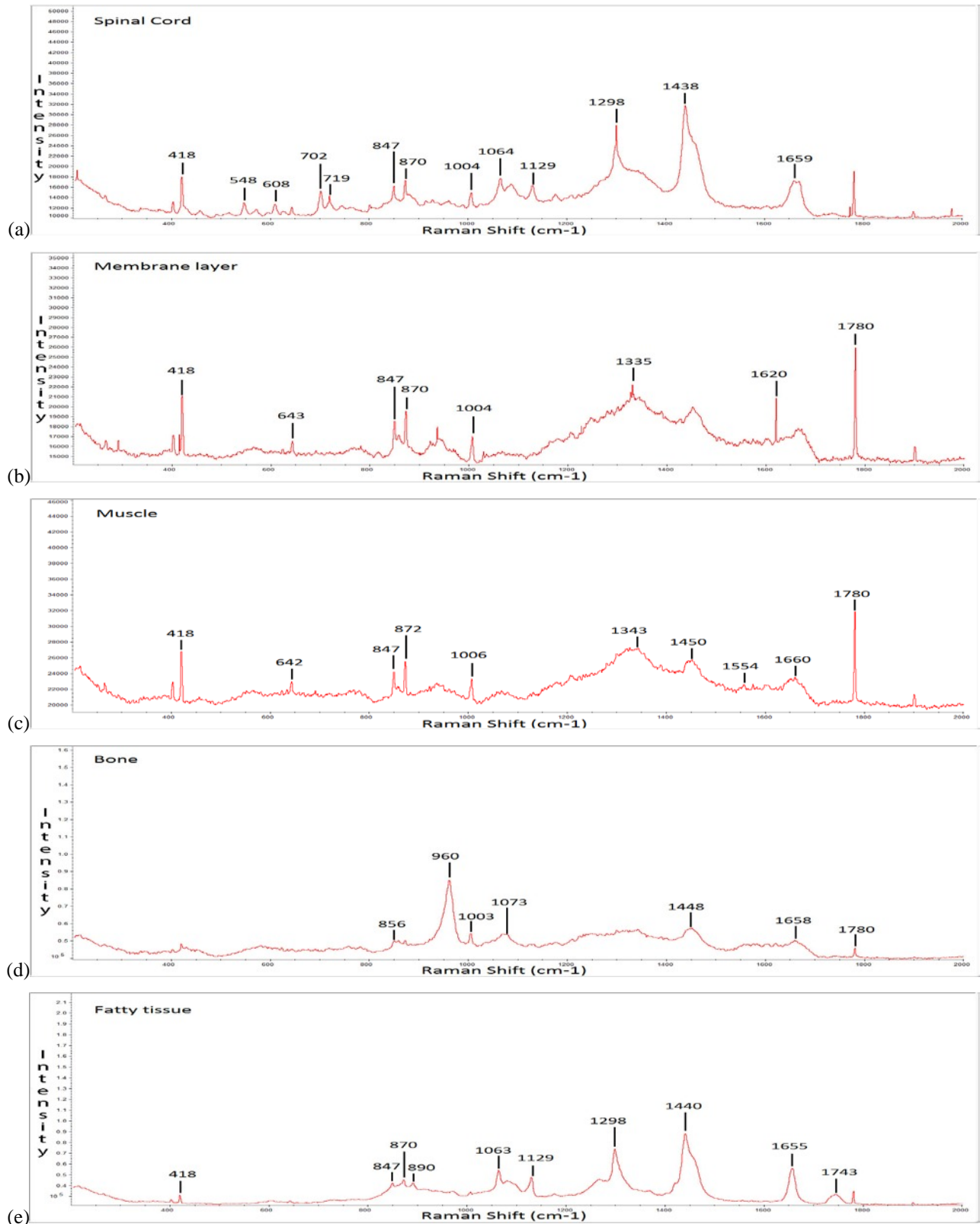
Figure 2. Average spectra of each category of samples, from top to bottom are the spinal cord, membrane layer of the spinal cord, muscle, bone and fatty tissue.

Table 1. Raman peak assignment

Raman Shift (cm-1)	Assignment	Reference
418, 548, 608, 702	Cholesterol, cholesterol ester	15
719	Symmetric stretch vibration of choline group characteristic for phospholipids	15
847	α-glucose, (C-O-C) skeletal mode	16
856, 870	C-C stretching, proline and hypro(collagen assignment)	17
960,1073	Calcium hydroxyapatite	18,23
1003	Phenylalanine, C-C skeletal	19
1004	vs (C-C), symmetric ring breathing, phenylalanine (protein assignment)	20
1063, 1064	Skeletal C-C stretch of lipids	21,22
1129	ν(C-C) skeletal of acyl backbone in lipid (trans conformation)	24
1298	Fatty acids; Acyl chains	15
1439, 1440	CH2 bending mode and deformation mode	25,17
1448	CH2,CH3 deformation	24
1450	CH2 bending (proteins)	26
1658, 1659	Amide I vibration (collagen like proteins)	26,22
1743	Lipid	27

Then, the average spectra of each category of samples are normalized to the same scale so that we can see the clear difference against each other. The results are shown in Figure 3 (on next page), from top to bottom are: spectrum of swine spinal cord, spectrum of membrane layer of the spinal cord, spectrum of muscle samples, spectrum of bone tissues and spectrum of fatty tissues. Compared with others, the spectrum of spinal cord has a distinctive region from about 400 to 800 cm^{-1} which is highlighted in a red circle. There are several featured peaks in this region that cannot be found in other samples' spectra, namely 548, 570, 608, 641, 702, and 719 cm^{-1}, which can be used to identify spinal cord against other samples. In the future study, multi-variates data analysis methods will be applied on the Raman spectral data, and a classification model will be built up for the task of spinal cord and spinal nerves identification.

4. SUMMARY

This paper presented the preliminary Raman microscope experiment on swine backbone tissue samples. Average spectra of the spinal cord, membrane layer of the spinal cord, muscle tissue, bone and fatty tissue are acquired and compared against each other. Peak assignments for each spectrum are made. The results show that the swine spinal cord has clear features in its spectrum compared with the spectra of adjacent tissues and these features can be used for spinal cord and spinal nerves identification.

Besides, a fiber-optic Raman sensing system was also introduced. Due to the laser source problems, the results of Raman sensing experiment were not presented. Future study will mainly focus on the fiber-optic Raman sensing system experiments and data analyzing algorithms.
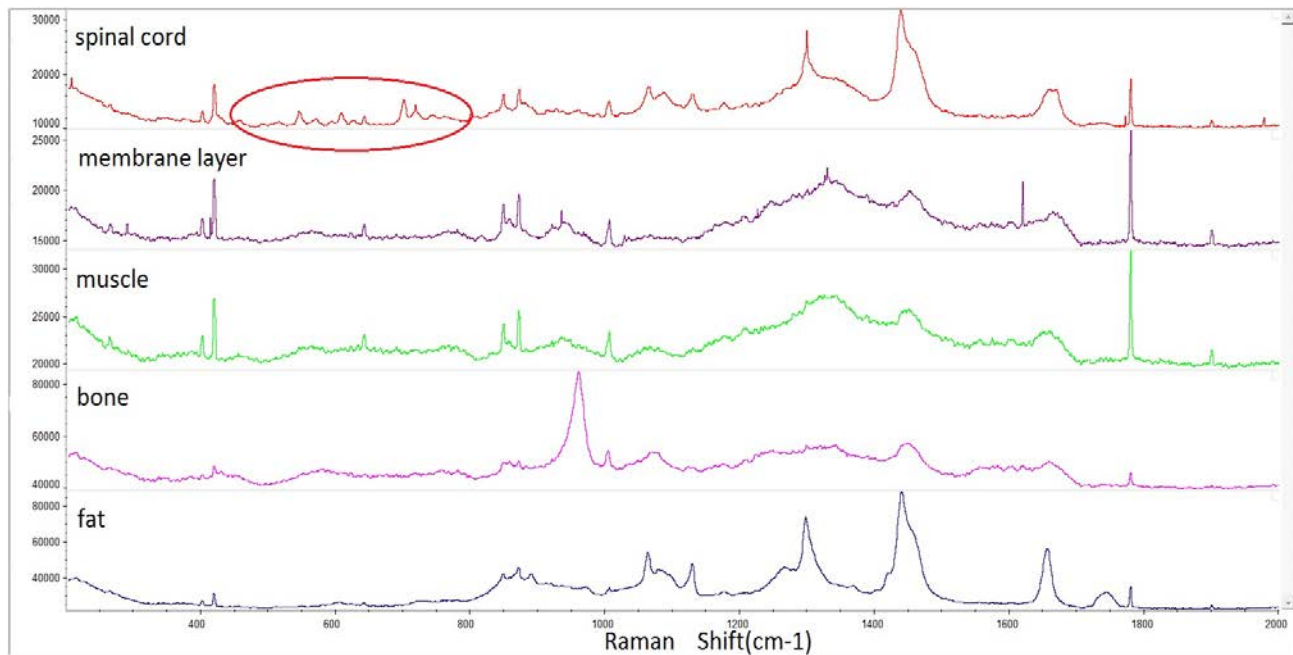
Figure 3. Spectral comparison of each category of samples, from top to bottom are: the spinal cord, membrane layer of the spinal cord, muscle tissue, bone and fatty tissue

ACKNOWLEDGEMENT

REFERENCES

[1] Bridwell, K. H., Lenke, L. G., Baldus, C., & Blanke, K., "Major intraoperative neurologic deficits in pediatric and adult spinal deformity patients," Incidence and etiology at one institution. Spine, 23(3), 324-331 (1998).

[2] O'Dowd, J. K., "Minimally invasive spinal surgery," Current Orthopaedics, 21(6), 442-450 (2007).

[3] Oppenheimer, J. H., DeCastro, I., & McDonnell, D. E., "Minimally invasive spine technology and minimally invasive spine surgery: a historical review," Neurosurgical focus, 27(3), E9 (2009).

[4] Westebring-Van Der Putten, E. P., Goossens, R. H. M., Jakimowicz, J. J., & Dankelman, J., "Haptics in minimally invasive surgery–a review," Minimally Invasive Therapy & Allied Technologies, 17(1), 3-16 (2008).

[5] Owen, J. H., Bridwell, K. H. Grubb, R., Jenny, A., Allen, B., Padberg, A. M., & Shimon, S. M., "The clinical application of neurogenic motor evoked potentials to monitor spinal cord function during surgery, " Spine, 16(8), S391 (1991).

[6] Nash JR, C. L., Lorig, R. A., Schatzinger, L. A., & Brown, R. H., "Spinal cord monitoring during operative treatment of the spine," Clinical orthopaedics and related research, 126, 100-105 (1977).

[7] Schmitt, M., & Popp, J., "Raman spectroscopy at the beginning of the twenty-first century," Journal of Raman Spectroscopy, 37(1-3), 20-28 (2006).

[8] Krafft, C., & Sergo, V., "Biomedical applications of Raman and infrared spectroscopy to diagnose tissues," Journal of Spectroscopy, 20(5-6), 195-218 (2006).

[9] Bergner, N., Bocklitz, T., Romeike, B. F., Reichart, R., Kalff, R., Krafft, C., & Popp, J., "Identification of primary tumors of brain metastases by Raman imaging and support vector machines," Chemometrics and Intelligent Laboratory Systems, 117, 224-232 (2012).

[10] Bergholt, M. S., Zheng, W., Lin, K., Ho, K. Y., Teh, M., Yeoh, K. G., & Huang, Z., "In vivo diagnosis of esophageal cancer using image-guided Raman endoscopy and biomolecular modeling," Technology in cancer research & treatment, 10(2), 103-112 (2011).

[11] Draga, R. O., Grimbergen, M. C., Vijverberg, P. L., Swol, C. F. V., Jonges, T. G., Kummer, J. A., & Ruud Bosch, J. L. H., "In vivo bladder cancer diagnosis by high-volume Raman spectroscopy," Analytical chemistry, 82(14), 5993-5999 (2010).

[12] Day, J. C., & Stone, N., "A subcutaneous Raman needle probe," Applied spectroscopy, 67(3), 349-354 (2013).

[13] Raman, C. V., & Krishnan, K. S., "A new type of secondary radiation," Nature, 121, 501-502 (1928).

[14] Huang, N., Short, M., Zhao, J., Wang, H., Lui, H., Korbelik, M., & Zeng, H., "Full range characterization of the Raman spectra of organs in a murine model," Optics express, *19*(23), 22892-22909 (2011).

[15] Krafft, C., Neudert, L., Simat, T., & Salzer, R., "Near infrared Raman spectra of human brain lipids," Spectrochimica Acta Part A: Molecular and Biomolecular Spectroscopy, 61(7), 1529-1535 (2005).

[16] Shetty, G., Kendall, C., Shepherd, N., Stone, N., & Barr, H., "Raman spectroscopy: elucidation of biochemical changes in carcinogenesis of oesophagus," British journal of cancer, 94(10), 1460-1464 (2006).

[17] Bonnier, F., & Byrne, H. J., "Understanding the molecular information contained in principal component analysis of vibrational spectra of biological systems," Analyst, 137(2), 322-332 (2012).

[18] Shim, M. G., Wong Kee Song, L. M., Marcon, N. E., & Wilson, B. C., "In vivo near-infrared Raman spectroscopy: demonstration of feasibility during clinical gastrointestinal endoscopy," Photochemistry and Photobiology, 72(1), 146-150 (2000).

[19] Chan, J. W., Taylor, D. S., Zwerdling, T., Lane, S. M., Ihara, K., & Huser, T., "Micro-Raman spectroscopy detects individual neoplastic and normal hematopoietic cells," Biophysical journal, 90(2), 648-656 (2006).

[20] Huang, Z., McWilliams, A., Lui, H., McLean, D. I., Lam, S., & Zeng, H., "Near-infrared Raman spectroscopy for optical diagnosis of lung cancer," International journal of cancer, 107(6), 1047-1052 (2003).

[21] Faolain, E. O., Hunter, M. B., Byrne, J. M., Kelehan, P., McNamara, M., Byrne, H. J., & Lyng, F. M., "A study examining the effects of tissue processing on human tissue sections using vibrational spectroscopy," Vibrational Spectroscopy, 38(1), 121-127 (2005).

[22] Stone, N., Kendall, C., Smith, J., Crow, P., & Barr, H., "Raman spectroscopy for identification of epithelial cancers," Faraday discussions, 126, 141-157 (2004).

[23] Silveira, L., Sathaiah, S., Zângaro, R. A., Pacheco, M. T., Chavantes, M. C., & Pasqualucci, C. A., "Correlation between near‐infrared Raman spectroscopy and the histopathological analysis of atherosclerosis in human coronary arteries," Lasers in surgery and medicine, 30(4), 290-297 (2002).

[24] Cheng, W. T., Liu, M. T., Liu, H. N., & Lin, S. Y., "Micro-Raman spectroscopy used to identify and grade human skin pilomatrixoma," Microscopy research and technique, 68(2), 75-79 (2005).

[25] Shafer‐Peltier, K. E., Haka, A. S., Fitzmaurice, M., Crowe, J., Myles, J., Dasari, R. R., & Feld, M. S., "Raman microspectroscopic model of human breast tissue: implications for breast cancer diagnosis in vivo," Journal of Raman Spectroscopy, 33(7), 552-563 (2002).

[26] Lakshmi, R. J., Kartha, V. B., Murali Krishna, C., R. Solomon, J. G., Ullas, G., & Uma Devi, P., "Tissue Raman spectroscopy for the study of radiation damage: brain irradiation of mice," Radiation research, 157(2), 175-182 (2002).

[27] Ronen, S. M., Stier, A., & Degani, H., "NMR studies of the lipid metabolism of T47D human breast cancer spheroids," FEBS letters, 266(1-2), 147-149 (1990).